COMPUTATIONAL CONTINUUM MECHANICS

ВЫЧИСЛИТЕЛЬНАЯ МЕХАНИКА СЛОШНЫХ СРЕД

Computational Continuum Mechanics. 2021. Vol. 14. No. 1. pp. 110-121 DOI: 10.7242/1999-6691/2021.14.1.10

NONLINEAR CONVECTION REGIMES OF A TERNARY MIXTURE IN A TWO-LAYER POROUS MEDIUM

N.A. Zubova[1] and T.P. Lyubimova[1,2]

[1]*Institute of Continuous Media Mechanics UB RAS, Perm, Russian Federation*
[2]*Perm National Research State University, Perm, Russian Federation*

Numerical experiments have been performed to study the onset and nonlinear regimes of convection of a ternary mixture of methane (35%), ethane (35%), and butane (30%) in a horizontally elongated rectangular region of a porous medium under the action of a geothermal gradient. The region has rigid, impermeable boundaries and is divided into two horizontal layers with equal porosity but different permeability and having the heights in ratio 1:3. The values of medium porosity and permeability are chosen close to those of real media, such as sands, sandstones or limestones. The components of the mixture belong to the main groups of chemical compounds present in oil and gas fields. The configuration under study is a model of hydrocarbon field. The calculations are carried out for the cases when the value of permeability of the upper layer is higher than that of the lower one and, conversely, when the lower layer is more permeable than the upper one. The rest of the parameters of the porous medium are considered to be the same in the entire computational domain. The problem is solved within the framework of the Darcy–Boussinesq model taking into account the effect of thermal diffusion. The temporal evolution of the local characteristics of the flow, the structure of the forming flow, and the distribution of the mixture components is evaluated. Analysis of the data shows that in the case of a more permeable narrow layer, the onset of convection has a local character. The flow arises in a more permeable layer and, as soon as convection develops, it begins to penetrate into a less permeable layer. However, the centers of the forming vortices are noticeably shifted towards the more permeable layer. Similar vortex displacements are observed in a thick layer with higher permeability, yet convection, in this case, is of the "large-scale" character.

Key words: convection, diffusion, thermal diffusion, hydrocarbon mixtures, porous medium

1. Introduction

Studies of multicomponent mixtures that saturate porous media are quite numerous and diverse in their applications [1–5]. The behavior of multicomponent mixtures in a porous medium presented in the literature is often studied without taking into account convection, or for a porous medium with homogeneous properties [6–10]. However, the analysis of oil and gas exploration data shows the presence of thermal anomalies that can be explained by thermal convection [11–14]. A large number of works are devoted to the separation of mixtures in a thermogravitational column filled with a porous medium [8, 15–17]. It follows from the results of these studies that convection significantly affects the distribution of mixture components.

A porous region, consisting of layers with different properties, usually appears in the problems of groundwater filtration, where interest, as a rule, is caused by the movement of the front of impurity concentration [18]. The structure of an oil-bearing formation is most often a certain, rather complex, tectonic form, where layers saturated with hydrocarbons with different porosity and permeability can alternate [19]. This, as well as the complex composition of the liquid that saturates the porous medium, are factors complicating the modeling.

Under the conditions of natural underground reservoirs (in the problems of underground filtration, hydrocarbon migration), it is becoming relevant to take into account the heterogeneity of the properties of the porous medium [20, 21], which can be described by the well-known Kozeny – Karman formula [22], which relates permeability to the porosity and particle size of the medium. In [23], direct numerical modeling of concentration convection in a liquid-saturated porous medium with anisotropic permeability, which is characterized by the ratio of vertical and horizontal permeabilities (permeability values across and along the study area), was carried out. The critical values of the wavenumber and Rayleigh number are determined for the Horton – Rogers – Lapwood problem with strong inhomogeneity and anisotropy in the case when the inhomogeneity is caused by the two-layer medium, and each of the constituent layers is homogeneous and isotropic in the horizontal plane [24].

Email addresses for correspondence: zubova.n@icmm.ru

In [18, 25–28], an inhomogeneous porous medium is modeled as a region consisting of layers of rocks with different values of porosity and permeability, and the properties of each layer are homogeneous. Such problems, often using topographic information and data on the degree of permeability of different types of rocks, are solved in the absence of thermal convection or under the assumption of a one-component or one-phase liquid saturating them [5, 18, 27, 29].

The aim of this work is to determine the effect of the non-uniformity of a porous medium in terms of permeability at constant porosity on nonlinear convection modes in a two-layer region. The configuration of the problem under consideration is a model of a hydrocarbon deposit, and consists of two horizontal layers of the same porosity and different permeability. A mixture of methane (35%), ethane (35%), and butane (30%) was used as a simulated mixture [30]. The components of the mixture are included in the main group of chemical compounds in the composition of the host rocks of oil and gas fields.

2. Problem statement and methods

Let us consider thermoconcentration convection of a three-component mixture in a horizontally elongated rectangular region of a porous medium with sides L and H ($L=5H$) saturated with a homogeneous three-component mixture. The area is divided into two horizontal layers in a ratio of 1: 3 in height (Fig. 1). All properties of the porous medium in the layers, with the exception of permeability, are the same.

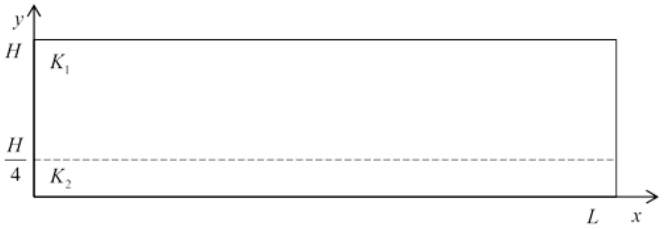

Fig. 1. Geometry of the problem.

To describe the composition of the mixture, we will use the vector of concentrations (mass fractions) $\boldsymbol{C}=(C_1,C_2)$, where C_1 and C_2 are the concentrations of the first and second components of the mixture (impurities), and $C_3=1-C_1-C_2$ is the concentration of the third component (solvent). We believe that the density of the mixture linearly depends on the temperature T and concentrations of its constituent components $\boldsymbol{C}$:

$$\rho=\rho_0(1-\beta_T(T-T_0)-\boldsymbol{I}\cdot\mathbf{B}(\boldsymbol{C}-\boldsymbol{C}_0)).$$

Here $\beta_T=-\frac{1}{\rho_0}\frac{\partial\rho}{\partial T}\Big|_C$ is coefficient of thermal expansion, $\mathbf{B}=\mathrm{diag}\{\beta_{C_1},\beta_{C_2}\}$ diagonal matrix of concentration expansion coefficients (such that $\beta_{C_i}=-\frac{1}{\rho_0}\frac{\partial\rho}{\partial C_i}\Big|_{T,\,C_j,\,j=1,\,2,\,j\neq i}$ $(i=1,2)$); $\boldsymbol{I}=(1,1)$, ρ_0, $\boldsymbol{C}_0=(C_{10},C_{20})$ and T_0 are the average values of density, concentration vector, and temperature of the mixture.

The unsteady equations of free thermoconcentration convection of a mixture in a porous medium in the framework of the Darcy – Boussinesq model taking into account the effect of thermal diffusion have the form [22]:

– in the top layer

$$0=-\frac{1}{\rho_0}\nabla p-\frac{\nu}{K_1}\boldsymbol{V}-\boldsymbol{g}\left(\beta_T\left(T-T_0\right)+\boldsymbol{I}\cdot\mathbf{B}\left(\boldsymbol{C}-\boldsymbol{C}_0\right)\right), \qquad (1)$$

$$\left(\rho c\right)^{*}\frac{\partial T}{\partial t}+\left(\rho c\right)_{f}\boldsymbol{V}\cdot\nabla T=\lambda^{*}\nabla^{2}T\,, \tag{2}$$

$$\varepsilon^{*}\frac{\partial \boldsymbol{C}}{\partial t}+\boldsymbol{V}\cdot\nabla\boldsymbol{C}=\mathbf{D}\nabla^{2}\boldsymbol{C}+\boldsymbol{C}_{0}\left(\boldsymbol{I}-\boldsymbol{C}_{0}\right)\boldsymbol{D}_{T}\nabla^{2}T\,, \tag{3}$$

$$\nabla\cdot\boldsymbol{V}=0; \tag{4}$$

– in the bottom layer

$$0=-\frac{1}{\rho_{0}}\nabla p-\frac{\nu}{K_{2}}\boldsymbol{V}-\boldsymbol{g}\left(\beta_{T}\left(T-T_{0}\right)+\boldsymbol{I}\cdot\mathbf{B}\left(\boldsymbol{C}-\boldsymbol{C}_{0}\right)\right), \tag{5}$$

$$\left(\rho c\right)^{*}\frac{\partial T}{\partial t}+\left(\rho c\right)_{f}\boldsymbol{V}\cdot\nabla T=\lambda^{*}\nabla^{2}T\,, \tag{6}$$

$$\varepsilon^{*}\frac{\partial \boldsymbol{C}}{\partial t}+\boldsymbol{V}\cdot\nabla\boldsymbol{C}=\mathbf{D}\nabla^{2}\boldsymbol{C}+\boldsymbol{C}_{0}\left(\boldsymbol{I}-\boldsymbol{C}_{0}\right)\boldsymbol{D}_{T}\nabla^{2}T\,, \tag{7}$$

$$\nabla\cdot\boldsymbol{V}=0\,. \tag{8}$$

Here: $\boldsymbol{V}$ is vector of filtration rate; p is pressure; $\boldsymbol{g}$ is vector of the gravity acceleration; t is time; K_1 and K_2 are permeability of the upper and lower layers, respectively; ν is kinematic viscosity; λ^{*} is effective thermal conductivity of the porous medium; $\left(\rho c\right)^{*}$ is effective heat capacity of the porous medium; $\left(\rho c\right)_{f}$ is heat capacity of the liquid; ε^{*} is porosity; $\mathbf{D}$ is matrix of molecular diffusion coefficients of the mixture; $\boldsymbol{D}_{T}$ is the vector of thermal diffusion coefficients. The equations are written under the assumption of constant viscosity and transfer coefficients and neglecting the effects of barodiffusion and diffusion thermal conductivity (the Dufour effect).

We assume that the area under study has solid boundaries that are impenetrable for matter. The lateral boundaries are thermally insulated, at the horizontal boundaries constant different temperatures are maintained, corresponding to heating from below.

Diagonalization of the matrix of molecular diffusion coefficients in the initial equations makes it possible to exclude cross diffusion effects and thereby reduce the number of governing parameters of the problem. This transformation in dimensional variables can be written as [31, 32]:

$$\boldsymbol{C}=\mathbf{M}\mathbf{Q}^{-1}\hat{\boldsymbol{C}}\,,\qquad \boldsymbol{D}_{T}=\mathbf{M}\mathbf{Q}^{-1}\hat{\boldsymbol{D}}_{T}\,. \tag{9}$$

Here $\mathbf{M}$ is a matrix, in the columns of which there are eigenvectors $m_i=\left(m_{i1},\,\mathrm{m}_{i2}\right)^{\mathrm{T}}$ of the matrix $\mathbf{D}$; $\mathbf{Q}=\mathrm{diag}\left\{q_1,\,q_2\right\}$ where $q_i=\beta_i^{-1}\left(\beta_1 m_{i1}+\beta_2 m_{i2}\right)$; the subscript «T» denotes a transposition operation.

Transformation (9) allows one to reduce equations (1) - (8) to a system with a diagonal matrix $\hat{\mathbf{D}}$, a concentration vector $\hat{\boldsymbol{C}}$, and a vector of thermal diffusion coefficients $\hat{\boldsymbol{D}}_{T}$:

– for top layer

$$0=\frac{1}{\rho_{0}}\nabla p-\frac{\nu}{K_{1}}\boldsymbol{V}-\boldsymbol{g}\left(\beta_{T}\left(T-T_{0}\right)+\boldsymbol{I}\cdot\mathbf{B}\left(\hat{\boldsymbol{C}}-\hat{\boldsymbol{C}}_{0}\right)\right), \tag{10}$$

$$\left(\rho c\right)^{*}\frac{\partial T}{\partial t}+\left(\rho c\right)_{f}\boldsymbol{V}\cdot\nabla T=\lambda^{*}\nabla^{2}T\,, \tag{11}$$

$$\varepsilon^{*}\frac{\partial \hat{\boldsymbol{C}}}{\partial t}+\boldsymbol{V}\cdot\nabla\hat{\boldsymbol{C}}=\hat{\mathbf{D}}\nabla^{2}\hat{\boldsymbol{C}}+\hat{\boldsymbol{C}}_{0}\left(\boldsymbol{I}-\hat{\boldsymbol{C}}_{0}\right)\hat{\boldsymbol{D}}_{T}\nabla^{2}T\,, \tag{12}$$

$$\nabla\cdot\boldsymbol{V}=0; \tag{13}$$

– for the bottom layer

$$0 = \frac{1}{\rho_0}\nabla p - \frac{\nu}{K_2}\boldsymbol{V} - \boldsymbol{g}\left(\beta_T\left(T - T_0\right) + \boldsymbol{I}\cdot\mathbf{B}\left(\hat{\boldsymbol{C}} - \hat{\boldsymbol{C}}_0\right)\right), \tag{14}$$

$$\left(\rho c\right)^* \frac{\partial T}{\partial t} + \left(\rho c\right)_f \boldsymbol{V}\cdot\nabla T = \lambda^*\nabla^2 T\,, \tag{15}$$

$$\varepsilon^* \frac{\partial \hat{\boldsymbol{C}}}{\partial t} + \boldsymbol{V}\cdot\nabla\hat{\boldsymbol{C}} = \hat{\mathbf{D}}\nabla^2\hat{\boldsymbol{C}} + \hat{\boldsymbol{C}}_0\left(\boldsymbol{I} - \hat{\boldsymbol{C}}_0\right)\hat{\boldsymbol{D}}_T\nabla^2 T\,, \tag{16}$$

$$\nabla\cdot\boldsymbol{V} = 0\,. \tag{17}$$

Let us choose as units of measurement: the height of the area H for the length; a/H for the speed, where $a = \lambda^*/\left(\rho c\right)_f$ is the effective thermal diffusivity; $H^2\left(\rho c\right)^*/\lambda^*$ for the time; $\rho_0 a\nu/K_1$ for the pressure; ΔT for the temperature deviation from the equilibrium value; $\hat{\boldsymbol{C}}_0\left(\hat{\boldsymbol{C}}_0 - 1\right)\Delta T\hat{\boldsymbol{D}}_T\left(\hat{\mathbf{D}}\right)^{-1}$ for the deviation of concentration from the equilibrium value. Equations (10) - (17) in dimensionless form take the form:

– for top layer

$$0 = -\nabla p - \boldsymbol{V} + \mathrm{Ra}\left(T + \hat{\boldsymbol{\psi}}\hat{\boldsymbol{C}}\right)\boldsymbol{k}\,, \tag{18}$$

$$\frac{\partial T}{\partial t} + \boldsymbol{V}\cdot\nabla T = \nabla^2 T\,, \tag{19}$$

$$\varepsilon\frac{\partial \hat{\boldsymbol{C}}}{\partial t} + \boldsymbol{V}\cdot\nabla\hat{\boldsymbol{C}} = \mathbf{Le}^{-1}\left(\nabla^2\hat{\boldsymbol{C}} - \boldsymbol{I}\nabla^2 T\right), \tag{20}$$

$$\nabla\cdot\boldsymbol{V} = 0\,; \tag{21}$$

– for the bottom layer

$$0 = -\frac{1}{\gamma}\nabla p - \boldsymbol{V} + \frac{1}{\gamma}\mathrm{Ra}\left(T + \hat{\boldsymbol{\psi}}\hat{\boldsymbol{C}}\right)\boldsymbol{k}\,, \tag{22}$$

$$\frac{\partial T}{\partial t} + \boldsymbol{V}\cdot\nabla T = \nabla^2 T\,, \tag{23}$$

$$\varepsilon\frac{\partial \hat{\boldsymbol{C}}}{\partial t} + \boldsymbol{V}\cdot\nabla\hat{\boldsymbol{C}} = \mathbf{Le}^{-1}\left(\nabla^2\hat{\boldsymbol{C}} - \boldsymbol{I}\nabla^2 T\right), \tag{24}$$

$$\nabla\cdot\boldsymbol{V} = 0\,. \tag{25}$$

Here $\mathrm{Ra} = K_1 g\beta_T H\Delta T/\left(a\nu\right)$ is an analogue of the Rayleigh number for a porous medium, which in what follows for brevity will be called the "Rayleigh number"; $\hat{\boldsymbol{\psi}} = -\hat{\boldsymbol{C}}_0\left(\boldsymbol{I} - \hat{\boldsymbol{C}}_0\right)\beta_T^{-1}\mathbf{B}\left(\hat{\mathbf{D}}\right)^{-1}\hat{\boldsymbol{D}}_T$ is vector of separation ratios, which characterizes the thermal diffusion properties of the mixture; $\varepsilon = \varepsilon^*\left(\rho c\right)_f/\left(\rho c\right)^*$ is normalized porosity; $\mathbf{Le} = a\left(\hat{\mathbf{D}}\right)^{-1}$ is a diagonal matrix of Lewis numbers such that $Le_{11} = a/\hat{D}_{11}$, $Le_{22} = a/\hat{D}_{22}$; $\boldsymbol{k}$ is unit vertical vector; $\gamma = K_1/K_2$ is the ratio of the permeabilities of the layers; for dimensionless variables, the previous designations are retained.

On all external boundaries, we set the conditions of impermeability and the absence of a diffusion flow of matter, on the external horizontal boundaries we will set the temperature, on the vertical boundaries is the absence of heat flux, on the boundary between the layers is equality of the x-components of velocity:

$$x = 0, \quad x = 5: \qquad V_x = 0, \qquad \frac{\partial T}{\partial x} = 0, \qquad \frac{\partial \hat{\boldsymbol{C}}}{\partial x} = 0; \tag{26}$$

$$y = 0: \quad V_y = 0, \quad T = 1, \quad \frac{\partial \hat{\boldsymbol{C}}}{\partial y} - \boldsymbol{I}\frac{\partial T}{\partial y} = 0; \tag{27}$$

$$y = 1: \quad V_y = 0, \quad T = 0, \quad \frac{\partial \hat{\boldsymbol{C}}}{\partial y} - \boldsymbol{I}\frac{\partial T}{\partial y} = 0; \tag{28}$$

$$y = H/4: \quad V_{1x} = V_{2x}. \tag{29}$$

We will restrict ourselves to considering two-dimensional flows. Let us introduce the stream function as $V_x = \partial\Psi/\partial y$, $V_y = -\partial\Psi/\partial x$. Equations (18) - (25), written in terms of the stream function, take the form:

– for top layer

$$\nabla^2\Psi = \mathrm{Ra}\left(\frac{\partial T}{\partial x} + \hat{\boldsymbol{\psi}}\frac{\partial \hat{\boldsymbol{C}}}{\partial x}\right), \tag{30}$$

$$\frac{\partial T}{\partial t} + \frac{\partial\Psi}{\partial y}\frac{\partial T}{\partial x} - \frac{\partial\Psi}{\partial x}\frac{\partial T}{\partial y} = \nabla^2 T, \tag{31}$$

$$\varepsilon\frac{\partial \hat{\boldsymbol{C}}}{\partial t} + \frac{\partial\Psi}{\partial y}\frac{\partial \hat{\boldsymbol{C}}}{\partial x} - \frac{\partial\Psi}{\partial x}\frac{\partial \hat{\boldsymbol{C}}}{\partial y} = \mathbf{Le}^{-1}\left(\nabla^2\hat{\boldsymbol{C}} - \boldsymbol{I}\nabla^2 T\right); \tag{32}$$

– for the bottom layer

$$\nabla^2\Psi = \mathrm{Ra}\left(\frac{\partial T}{\partial x} + \hat{\boldsymbol{\psi}}\frac{\partial \hat{\boldsymbol{C}}}{\partial x}\right), \tag{33}$$

$$\frac{\partial T}{\partial t} + \frac{\partial\Psi}{\partial y}\frac{\partial T}{\partial x} - \frac{\partial\Psi}{\partial x}\frac{\partial T}{\partial y} = \nabla^2 T, \tag{34}$$

$$\varepsilon\frac{\partial \hat{\boldsymbol{C}}}{\partial t} + \frac{\partial\Psi}{\partial y}\frac{\partial \hat{\boldsymbol{C}}}{\partial x} - \frac{\partial\Psi}{\partial x}\frac{\partial \hat{\boldsymbol{C}}}{\partial y} = \mathbf{Le}^{-1}\left(\nabla^2\hat{\boldsymbol{C}} - \boldsymbol{I}\nabla^2 T\right). \tag{35}$$

Boundary conditions (26) - (29) in terms of the stream function look like this:

$$x = 0, \quad x = 5: \quad \Psi = 0, \quad \frac{\partial T}{\partial x} = 0, \quad \frac{\partial \hat{\boldsymbol{C}}}{\partial x} = 0; \tag{36}$$

$$y = 0: \quad \Psi = 0, \quad T = 1, \quad \frac{\partial \hat{\boldsymbol{C}}}{\partial y} - \boldsymbol{I}\frac{\partial T}{\partial y} = 0; \tag{37}$$

$$y = 1: \quad \Psi = 0, \quad T = 0, \quad \frac{\partial \hat{\boldsymbol{C}}}{\partial y} - \boldsymbol{I}\frac{\partial T}{\partial y} = 0; \tag{38}$$

$$y = 1/4: \quad \frac{\partial\Psi_1}{\partial y} = \gamma\frac{\partial\Psi_2}{\partial y}. \tag{39}$$

At the initial moment of time, the temperature and concentration of the mixture components are assumed to be linearly dependent on the vertical coordinate (heating from below).

Problem (30) - (39) was solved numerically using the finite difference method. Spatial derivatives were approximated by central differences. The unsteady equations were reduced to a

discrete form using an explicit finite-difference scheme with a constant time step equal to $h_t = h^2/16$, where h is the space step. The stream function was found from the Poisson equation by the method of successive upper relaxation.

The vertical size of the computational domain was 100 m. In both layers, the porosity values were the same and were assumed to be equal $\varepsilon = 0,2$. The temperature difference between the upper and lower boundaries of the computational domain corresponded to the average value of the geothermal gradient $3 \cdot 10^{-2}$ K/m. Thermal and physical properties of a mixture of methane, ethane and butane (at $T_0 = 315$ K, $p = 7,0 \cdot 10^6$ Pa) are presented in the table. Additional calculations showed that in the case of a single-layer porous medium with height H the threshold value of the Rayleigh number is $\mathrm{Ra} \approx 1,3$. The values of the permeability of the medium in one layer of the two-layer region in all calculations were recorded and equal to $2,9 \cdot 10^{-15}$ m^2, which corresponds to the Rayleigh number $\mathrm{Ra} = 1$ for the layer height H. In this case, convection did not occur. In the other layer, the permeability value varied and was 10, 30 or 50 times higher. Calculations were carried out for the ratios: $\gamma > 1$ and $\gamma < 1$. The selected values of porosity and permeability correspond to the data for sands, limestones, shales [33, 34].

Table. Physical properties of the mixture [30].

ρ_0, kg/m^3	450,35	$D_{11} \times 10^9$, m^2/s	3,14
β_T, K^{-1}	–0,52×10^{-2}	$D_{12} \times 10^9$, m^2/s	–0,77
β_{C_1}	–1,25	$D_{21} \times 10^9$, m^2/s	–0,32
β_{C_2}	–0,72	$D_{22} \times 10^9$, m^2/s	4,68
ν, m^2/s	4,44×10^{-7}	$D_1^T \times 10^{12}$, m^2/(s·K)	–5,13
a, m^2/s	10^{-7}	$D_2^T \times 10^{12}$, m^2/(s·K)	–1,35

3. Numerical results

For the three-component mixture of methane, ethane, and butane considered in this paper, the values of the dimensionless parameters transformed after the procedure of matrix diagonalization in (9) were: $\psi_1 = 2,4 \cdot 10^{-3}$, $\psi_2 = 0,427$, $Le_{11} = 20,7$, $Le_{22} = 33,4$. The separation ratios of the components of the mixture ψ_1 and ψ_2 are positive; therefore, when heated from below, the lighter components of the mixture (methane and ethane) under the action of thermal diffusion accumulate near the heated lower boundary of the studied region, and the heavy component of the mixture, butane, near the cold upper boundary.

Let's start our analysis with a case $\gamma < 1$. In this case, convection should occur in the lower layer, where the permeability is higher, and in the course of time penetrate into the upper layer. Figure 2a

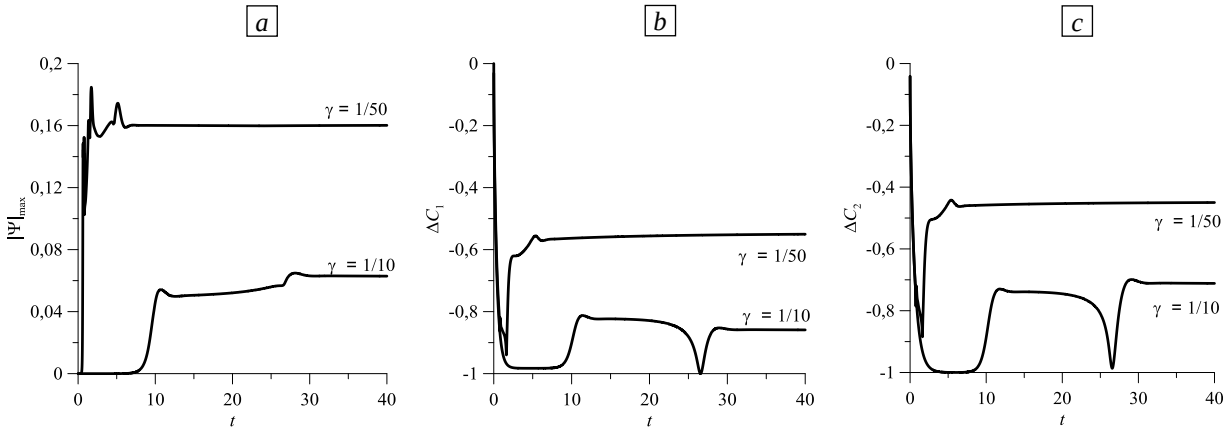

Fig. 2. Time evolution of the maximum value of the modulus of the stream function in the region (a) and the difference in the concentrations of the first (b) and second (c) components of the mixture between the centers of the upper and lower boundaries of the region; $\gamma < 1$.

shows the time evolution of the maximum value of the modulus of the stream function. As can be seen, in the range of values of the Rayleigh numbers corresponding to the inequality $\gamma < 1$, the same type of development of convection is realized. First, a certain non-convective period is observed (the stream function is practically zero), the duration of which decreases with decreasing value γ. The onset of convection is accompanied by a sharp jump in traffic intensity. Then, through a series of rearrangements, which are also characterized by jumps in the traffic intensity, the stationary regime is reached. The traffic intensity in a stationary mode increases with decreasing ratio γ.

Figure 3 shows the structure of the steady flow and the distribution of the impurity concentration for the case of $\gamma = 1/50$. Stationary motion in the corresponding range of values has a four-vortex shape (Fig. 3a), the centers of the formed vortices are displaced into a layer with a higher permeability. A change in the curvature of the isolines is observed near the boundary of the layers (Fig. 3a – c).

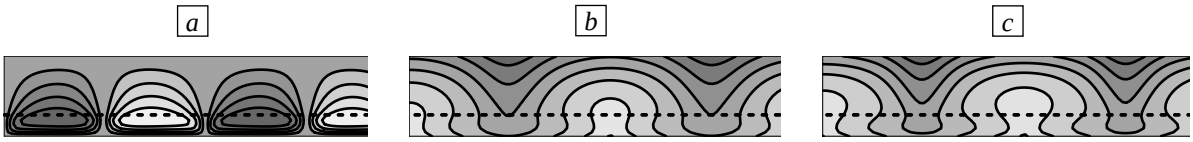

Fig. 3. Isolines of the stream function (a) and the concentration of the first (b) and second (c) components of the mixture at the time moment of $t = 40$ for the case of $\gamma = 1/50$.

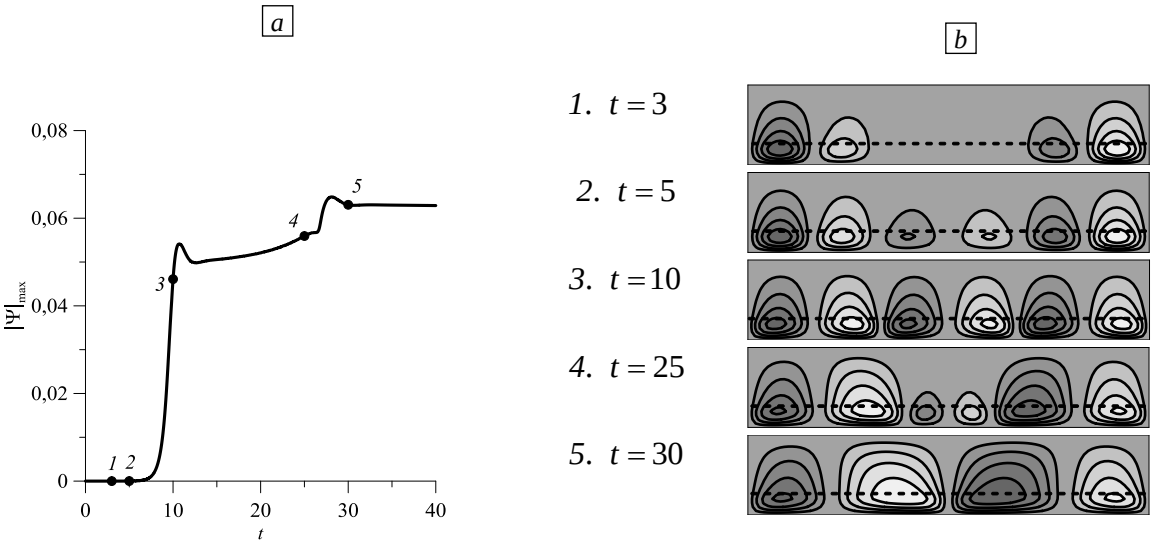

Fig. 4. Time evolution of the maximum value of the modulus of the stream function c in a two-layer porous region (a) and the isolines of the stream function at different times (b); $\gamma = 1/10$.

Let us consider the process of formation of a four-vortex stationary flow using the $\gamma = 1/10$ relationship example. Additional calculations showed that for a single layer with parameters corresponding to a thin lower layer (aspect ratio is 20:1, height is 25 m, permeability is $5{,}16 \cdot 10^{-15}$ m^2), the wavelength of the most dangerous disturbances is $\lambda \approx 0{,}8$, and for a single layer with parameters (aspect ratio is 5:1, height is 100 m, permeability is $5{,}84 \cdot 10^{-13}$ m^2) is $\lambda \approx 1{,}25$. As follows from Figure 4, even in the non-convective period near the lateral boundaries of the region, convective vortices are beginning to form, a weak flow penetrates into the upper layer, which has a lower permeability: here one can see the "local" onset of convection [22, 35, 36] (Fig. 4*a*, points *1*, *2*; Fig.4*b* $t = 3$, $t = 5$). With the development of instability, the number of vortices increases so that at $t = 10$ (Fig. 4*b*) a six-vortex flow (wavelength is $\lambda \approx 0{,}8$) is observed in the region, which also passes into the upper layer: convection becomes "large-scale". After the first peak of the traffic

intensity (Fig. 4*a*), the two central vortices decrease and disappear (Fig. 4*b*, $t=25$, $t=30$), and the motion turns into a four-vortex (wavelength is $\lambda \approx 1,25$).

Fig. 5. Isolines of the stream function (*a*) and the concentration distribution of the first component of the mixture (*b*) at the time instant $t=1$ at $\gamma = 1/50$.

More clearly "local" convection is demonstrated in Fig. 5 for the case $\gamma = 1/50$. At the time moment $t=1$, a multi-vortex motion takes place in the layer with higher permeability, which is almost not manifested in the rest of the region (Fig. 5a). Isolines of the concentration of the first component of the mixture are also strongly deformed only in this layer (Fig. 5b). Over time, movement penetrates into the upper part of the area (see Fig. 3).

In the case of $\gamma > 1$, convection appears in the upper layer with a high permeability value and gradually captures the lower layer. As can be seen from Fig. 6, at small times, here, as in the case of $\gamma < 1$, there is a non-convective period (Fig. 6a), during which a close to purely diffusion separation of the mixture components occurs (Fig. 6b, c). At a certain moment in time, convection is formed, accompanied by a strong jump in the intensity of movement, then an oscillatory exit to a stationary mode is observed (Fig. 6 a). As can be seen from the comparison of Figures 2 and 6, the time of the onset of convection is much shorter, and its intensity is much higher at $\gamma > 1$, that is, at the capture of a higher upper layer by convection.

The steady-state flow at $\gamma > 1$ has a multi-vortex shape, and the spatial scale of the vortices decreases with an increase in the permeability of the upper layer. So, at $\gamma = 10$ and $\gamma = 30$ the flow structure turns out to be four-vortex, which is shown in Fig. 6a for $\gamma = 10$ as an example, and at $\gamma = 50$ the number of vortices increases to six (Fig. 8a). The concentration contours of the mixture components are significantly deformed by a complex intense flow (Fig. 7b, c); the degree of their deformation increases with γ increasing (Fig. 8b, c). As can be seen from Figures 7 and 8, the displacement of the flow towards a more permeable layer is extremely weak, in contrast to the $\gamma < 1$ case, which is explained both by the relative height of the layer in which convection occurs, and by the gravitational mechanism of its development.

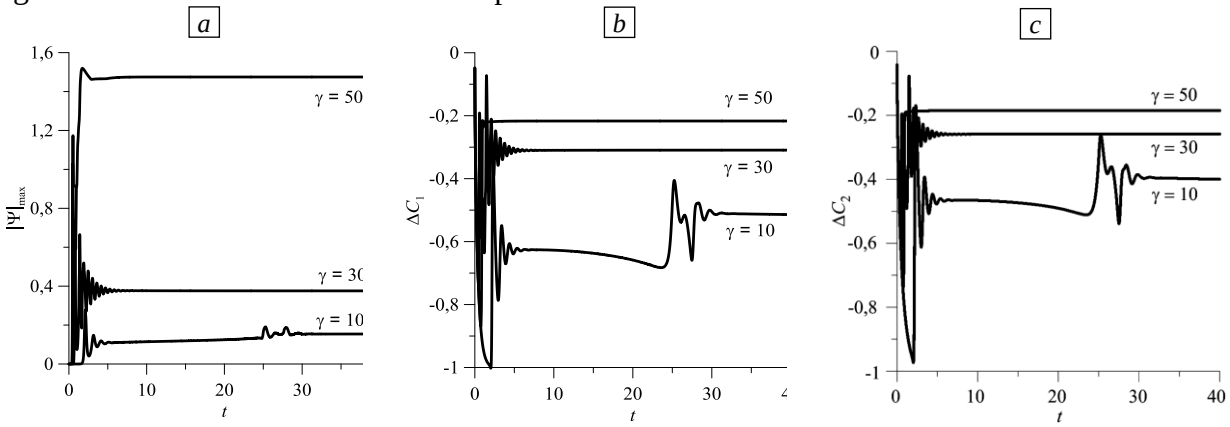

Fig. 6. Time evolution of the maximum value of the modulus of the stream function in the region (a) and the difference in the concentrations of the first (b) and second (c) components of the mixture between the centers of the upper and lower boundaries; $\gamma > 1$.

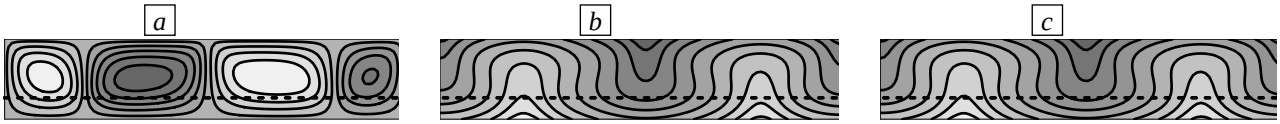

Fig. 7. Isolines of the stream function (a) and the concentration of the first (b) and second (c) components of the mixture at the moment of time $t = 40$ for $\gamma = 10$

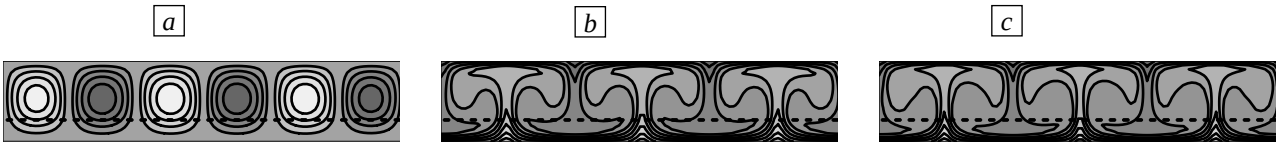

Fig. 8. Isolines of the stream function (a) and the concentration of the first (b) and second (c) components of the mixture at the moment of time $t = 40$ for $\gamma = 50$

b

The convective flow at $\gamma > 1$, as in the previous case, is formed near the lateral boundaries (Fig. 9*a*, point *1*, Fig. 9*b*). Since the layer in which the flow arises occupies most of the computational domain, the effect of the initiation of "local" convection is very weak: the motion almost immediately penetrates into the layer with a lower permeability (Fig. 9b – f). The motion formed at short times at $\gamma = 10$ has an eight-vortex shape. As can be seen in Figs 6a and 9a, for these values of γ over time $t \approx 23-30$, jumps in the flow intensity are observed. Figure 9g – k shows the restructuring of the flow in this time range: some vortices merge, and the flow becomes four-vortex.

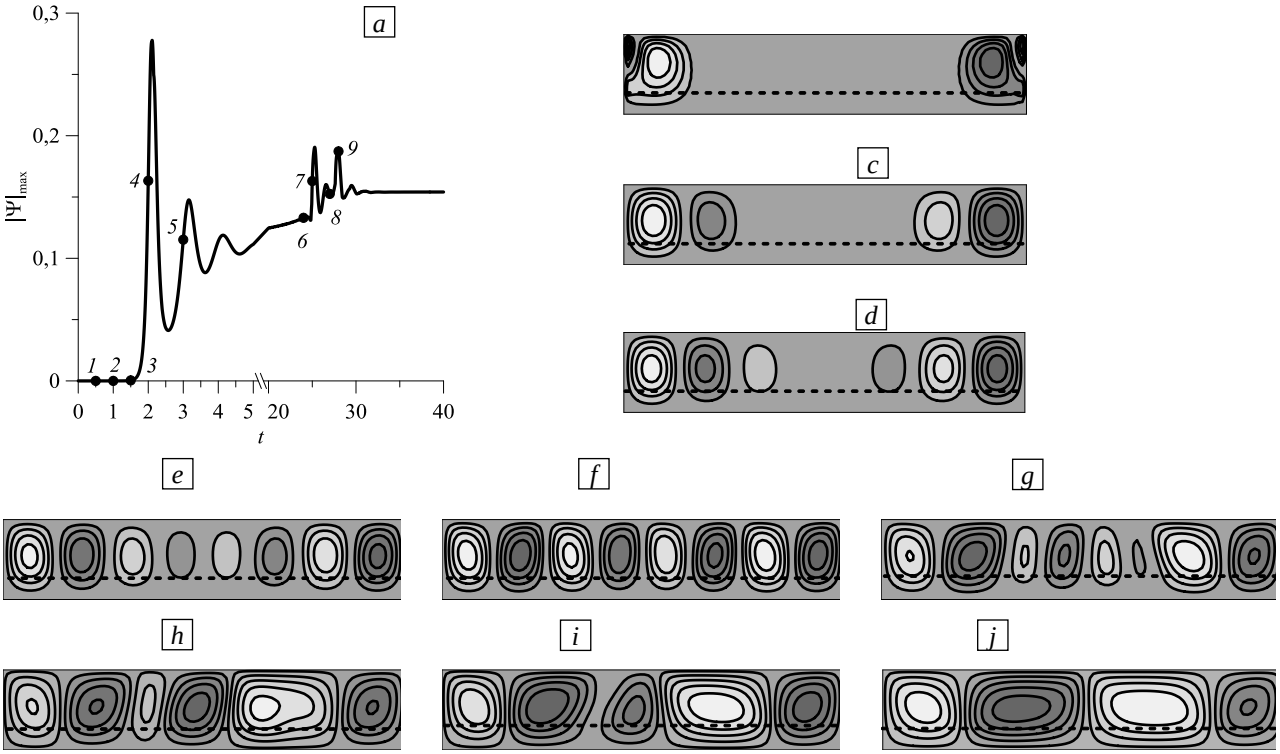

Fig. 9. A fragment of the time evolution of the maximum value of the stream function modulus in region (a) and the evolution of the stream function structure with time: (*b*) $t = 0{,}5$ (point *1*); (*c*) $t = 1$ (*2*); (*d*) $t = 1{,}5$ (*3*); (*e*) $t = 2$ (*4*); (*f*) $t = 3$ (*5*); (*g*) $t = 24$ (*6*); (*h*) $t = 25$ (*7*); i) $t = 27$ (*8*); (*j*) $t = 28$ (*9*); $\gamma = 10$.

When the value γ is increased to 30, the formation of motion occurs in a similar way, but the entire process of its restructuring from eight-vortex to four-vortex is beginning immediately after the onset. In this case, on the graph of the time evolution of the maximum value of the modulus of the stream function, damped oscillations are observed (Fig. 6a). With a further increase in the Rayleigh number in the layer with higher permeability up to the value of $\gamma = 50$, the motion does not undergo such transformations.

4. Conclusion

The emergence and nonlinear modes of convection of a three-component mixture of methane (35%), ethane (35%), and butane (30%) in a horizontally elongated rectangular region of a porous medium are numerically investigated. The area in a ratio of 1: 3 is divided in height into two horizontal layers with equal porosity, but differing in permeability. Thus, the investigated configuration of the computational domain of the problem is a model of a hydrocarbon deposit. The cases are analyzed when the value of the upper layer permeability is higher than that of the lower one, and, conversely, the lower layer is more permeable than the upper one. The rest of the parameters of the porous medium are considered the same. The problem is solved within the framework of the Darcy – Boussinesq model.

The results of numerical simulation show that the formation of a steady flow is observed in the entire considered range of parameters. The steady-state flow structure is four-vortex with a more permeable lower layer and a small permeability ratio in a more permeable upper layer. With an increase in the permeability ratio, in the second case, the spatial scale of the convective flow decreases: it becomes six-vortex. The time for the onset of convection in the more permeable upper layer is shorter, and the intensity of the established flow is much higher than in the more permeable lower layer. As a result, the maximum separation of the components of the mixture is less with a more permeable upper layer.

The "local" nature of the onset of convection in the investigated two-layer configuration is shown. This effect is most clearly manifested in a more permeable thin lower layer. During the development of convection, the flow begins to penetrate into the less permeable upper layer, but the centers of the forming vortices noticeably shift towards the more permeable layer. A similar displacement of vortices occurs with a more permeable thick upper layer. However, in this case, the onset of convection has a "large-scale" character. Such differences can be explained by the gravitational mechanism of convection.

This work was carried out with the financial support of the Russian Science Foundation (grant no. 20-71-00147).

References

1. Lyubimova TP., Lepikhin A.P., Parshakova Ya.N., Tsiberkin K.B. Numerical modeling of liquid waste infiltration from storage facilities into surrounding groundwater and surface water bodies. *Vychisl. mekh. splosh. sred – Computational Continuum Mechanics*, 2015, vol. 8, no. 3, pp. 310-318. http://dx.doi.org/10.7242/1999-6691/2015.8.3.26
2. Lyubimova T.P., Lyubimov D.V., Baydina D.T., Kolchanova E.A., Tsiberkin K.B. Instability of plane-parallel flow of incompressible liquid over a saturated porous medium. *Phys. Rev. E*, 2016, vol. 94, 013104. http://dx.doi.org/10.1103/PhysRevE.94.013104
3. Collell J., Galliero G., Vermorel R., Ungerer P., Yiannourakou M., Montel F., Pujol M. Transport of multicomponent hydrocarbon mixtures in shales organic matter by molecular simulations. *J. Phys. Chem. C*, 2015, vol. 119, pp. 22587-22595. http://dx.doi.org/10.1021/acs.jpcc.5b07242

4. Maryshev B., Lyubimova T., Lyubimov D. Two-dimensional thermal convection in porous enclosure subjected to the horizontal seepage and gravity modulation. *Phys. Fluid.*, 2013, vol. 25, 084105. http://dx.doi.org/10.1063/1.4817375
5. Barvier E. Geothermal energy technology and current status: an overview. *Renew. Sustain. Energ. Rev.*, 2002, vol. 6, pp. 3-65. https://doi.org/10.1016/S1364-0321(02)00002-3
6. Charrier-Mojtabi M.C., Elhajjar B., Mojtabi A. Analytical and numerical stability analysis of Soret-driven convection in a horizontal porous layer. *Phys. Fluid.*, 2007, vol. 19, 124104. https://doi.org/10.1063/1.2821460
7. Ryzhkov I.I., Shevtsova V.M. On thermal diffusion and convection in multicomponent mixtures with application to the thermogravitational column. *Phys. Fluid.*, 2007, vol. 19, 027101. https://doi.org/10.1063/1.2435619
8. Benano-Melly L.B., Caltagirone J.-P., Faissat B., Montel F., Costeseque P. Modeling Soret coefficient measurement experiments in porous media considering thermal and solutal convection. *Int. J. Heat Mass Tran.*, 2001, vol. 44, pp. 1285-1297. https://doi.org/10.1016/S0017-9310(00)00183-6
9. Lyubimova T., Zubova N. Nonlinear regimes of the Soret-induced convection of ternary fluid in a square porous cavity. *Transp. Porous Med.*, 2019, vol. 127, pp. 559-572. https://doi.org/10.1007/s11242-018-1211-2
10. *Lyubimova T.P., Zubova N.A.* Onset and nonlinear regimes of convection of ternary mixture in a rectangular porous cavity taking into account Soret effect. *Vychisl. mekh. splosh. sred – Computational Continuum Mechanics*, 2019, vol. 12, no. 3, pp. 249-262. https://doi.org/10.7242/1999-6691/2019.12.3.21
11. Bonté D., Van Wees J.-D., Verweij J.M. Subsurface temperature of theonshore Netherlands: new temperature dataset and modelling. *Geol. Mijnbouw*, 2012, vol. 91, pp. 491-515. https://doi.org/10.1017/S0016774600000354
12. Pasquale V., Chiozzi P., Verdoya M. Evidence for thermal convection in the deep carbonate aquifer of the eastern sector of the Po Plain, Italy. *Tectonophysics*, 2013, vol. 594, pp. 1-12. https://doi.org/10.1016/j.tecto.2013.03.011
13. Guillou-Frottier L., Carré C., Bourgine B., Bouchot V., Genter A. Structure of hydrothermal convection in the Upper Rhine Graben as inferred from corrected temperature data and basin-scale numerical models. *J. Volcanol. Geoth. Res.*, 2013, vol. 256, pp. 29-49. https://doi.org/10.1016/j.jvolgeores.2013.02.008
14. Lipsey L., Pluymaekers M., Goldberg T., van Oversteeg K., Ghazaryan L., Cloetingh S., van Wees J.-D. Numerical modelling of thermal convection in the Luttelgeest carbonate platform, the Netherlands. *Geothermics*, 2016, vol. 64, pp. 135-151. https://doi.org/10.1016/j.geothermics.2016.05.002
15. Nasrabadi H., Hoteit H., Firoozabadi A. An analysis of species separation in thermogravitational column filled with porous media. *Transp. Porous Med.*, 2007, vol. 67, pp. 473-486. https://doi.org/10.1007/s11242-006-9037-8
16. Larabi M.A., Mutschler D., Mojtabi A. Thermal gravitational separation of ternary mixture n-dodecane/isobutylbenzene/tetralin components in a porous medium. *J. Chem. Phys.*, 2016, vol. 144, 244902. https://doi.org/10.1063/1.4954244
17. Abahri O., Sadaoui D., Mansouri K., Mojtabi A., Mojtabi M.C. Thermogravitational separation in horizontal annular porous cell. *Mechanics & Industry*, 2017, vol. 18, 106. https://doi.org/10.1051/meca/2015115
18. Soboleva E. Density-driven convection in an inhomogeneous geothermal reservoir. *Int. J. Heat Mass Tran.*, 2018, vol. 127, pp. 784-798. https://doi.org/10.1016/j.ijheatmasstransfer.2018.08.019
19. Gubkin I.M. *Ucheniye o nefti* [The doctrine of oil]. Moscow, Nauka, 1975. 387 p.
20. Wangen M., Throndsen T. Simple 3-D modeling of hydrocarbon migration. *Multidimensional basin modeling*, ed. S. Du¨ppenbecker, R. Marzi. AAPG/Datapages Discovery Series, 2003. Pp. 243-253.

21. Wen B., Akhbar D., Zhang L., Hesse M.A. Convective carbon dioxide dissolution in a closed porous medium at low pressure. *J. Fluid Mech.*, 2018, vol. 854, pp. 56-87. https://doi.org/10.1017/jfm.2018.622
22. Nield D.A., Bejan A. *Convection in porous media*. Springer, 2013. 778 p. https://doi.org/10.1007/978-1-4614-5541-7
23. De Paoli M., Zonta F., Soldati A. Dissolution in anisotropic porous media: Modelling convection regimes from onset to shutdown. *Phys. Fluid.*, 2017, vol. 29, 026601. https://doi.org/10.1063/1.4975393
24. Nield D.A., Kuznetsov A.V. The onset of convection in an anisotropic heterogeneous porous medium: A new hydrodynamic boundary condition. *Transp. Porous Med.*, 2019, vol. 127, pp. 549-558. https://doi.org/10.1007/s11242-018-1210-3
25. Soboleva E. Numerical investigations of haline-convective flows of saline groundwater. *J. Phys. Conf. Ser.*, 2017, vol. 891, 012104. https://doi.org/10.1088/1742-6596/891/1/012104
26. Soboleva E. Numerical simulation of haline-convection in geothermal reservoirs. *J. Phys. Conf. Ser.*, 2017, vol. 891, 012105. https://doi.org/10.1088/1742-6596/891/1/012105
27. Zech A., Zehner B., Kolditz O., Attinger S. Impact of heterogeneous permeability distribution on the groundwater flow systems of a small sedimentary basin. *J. Hydrol.*, 2016, vol. 532, pp. 90-101. https://doi.org/10.1016/j.jhydrol.2015.11.030
28. Salibindla A.K.R., Subedi R., Shen V.C., Masuk A.U.M., Ni R. Dissolution-driven convection in a heterogeneous porous medium. *J. Fluid Mech.*, 2018, vol. 857, pp. 61-79. https://doi.org/10.1017/jfm.2018.732
29. Kocberber S., Collins R.E. *SPE Annual Technical Conference and Exhibition. New Orleans, Louisiana, September 23-26, 1990. Pp. 175-201*. https://doi.org/10.2118/20547-MS
30. Ghorayeb K., Firoozabadi A. Modeling multicomponent diffusions and convection in porous media. *SPE J.*, 2000, vol. 5, pp. 158-171. https://doi.org/10.2118/62168-PA
31. Ryzhkov I.I. *Termodiffuziya v smesyakh: uravneniya, simmetrii, resheniya i ikh ustoychivost'* [Thermal diffusion in mixtures: equations, symmetries and solutions and their stability]. Novosibirsk: Izd-vo SO RAN, 2013. 215 p.
32. Lyubimova T., Zubova N. Onset and nonlinear regimes of ternary mixture convection in a square cavity. *Eur. Phys. J. E*, 2015, vol. 38, 19. https://doi.org/10.1140/epje/i2015-15019-2
33. Forster S., Bobertz B., Bohling B. Permeability of sands in the coastal areas of the southern Baltic Sea: mapping a grain-size related sediment property. *Aquatic Geochemistry*, 2003, vol. 9, pp. 171-190. https://doi.org/10.1023/B:AQUA.0000022953.52275.8b
34. Iscan A.G., Kok M.V. Porosity and permeability determinations in sandstone and limestone rocks using thin section analysis approach. *Energy Sources, Part A*, 2009, vol. 31, pp. 568-575. https://doi.org/10.1080/15567030802463984
35. McKibbin R., O'Sullivan M.J. Onset of convection in a layered porous medium heated from below. *J. Fluid Mech.*, 1980, vol. 96, pp. 375-393. https://doi.org/10.1017/S0022112080002170
36. McKibbin R., O'Sullivan M.J. Heat transfer in a layered porous medium heated from below. *J. Fluid Mech.*, 1981, vol. 111, pp. 141-173. https://doi.org/10.1017/S0022112081002334

The authors declare no conflict of interests.

The paper was received on 06.04.2021.
The paper was accepted for publication on 28.04.2021.